Doping-driven antiferromagnetic insulator-superconductor transition:
A quantum Monte Carlo study

Tianxing Ma [1,2,*] Da Wang,[3,*] and Congjun Wu [4,5,6,7,†]

[1]*Department of Physics, Beijing Normal University, Beijing 100875, China*
[2]*Department of Physics, University of California, San Diego, California 92093, USA*
[3]*National Laboratory of Solid State Microstructures & School of Physics, Nanjing University, Nanjing 210093, China*
[4]*Department of Physics, School of Science, Westlake University, Hangzhou 310024, Zhejiang, China*
[5]*Institute for Theoretical Sciences, Westlake University, Hangzhou 310024, Zhejiang, China*
[6]*Key Laboratory for Quantum Materials of Zhejiang Province, School of Science, Westlake University, Hangzhou 310024, Zhejiang, China*
[7]*Institute of Natural Sciences, Westlake Institute for Advanced Study, Hangzhou 310024, Zhejiang, China*

How superconductivity emerges in the vicinity of an antiferromagnetic insulating state is a long-standing issue of strong correlation physics. We study the transition from an antiferromagnetic insulator to a superconductor by hole doping based on a bilayer generalization of a Hubbard model. The projector quantum Monte Carlo simulations are employed, which are sign problem free both at and away from half filling. An anisotropic Ising antiferromagnetic Mott insulating phase occurs at half filling, which is weakened by hole doping. Below a critical doping value, antiferromagnetism coexists with the singlet superconductivity, which is a pairing across each rung with an extended *s*-wave symmetry. As doping further increases, the antiferromagnetic order vanishes, leaving only a superconducting phase. These results provide important information on how superconductivity appears upon doping the parent Mott-insulating state.

I. INTRODUCTION

The study on strongly correlated electron systems is a central topic of condensed matter physics for exploring novel states of matter. In the vicinity of the antiferromagnetic (AF) insulating phase, unconventional superconducting (SC) states appear by doping or applying pressure to systems of heavy-fermion materials [1], high T_c cuprates [2], iron pnictides [3], and organic superconductors [4]. In the past several decades, the doped Mott insulators and the consequential competitions among antiferromagnetism, superconductivity, and charge orderings have been extensively studied with significant efforts from various different perspectives [5–13].

How superconductivity arises by doping Mott insulators is an outstanding problem of condensed matter physics. Due to its nonperturbative nature, sufficiently accurate numerical methods are essential to resolve small energy differences among competing orders [11–14]. Nevertheless, exact diagonalizations are limited to small system sizes due to the exponential growth of the many-body Hilbert space [15]. The density-matrix-renormalization group [16] and tensor-network methods [17] have been successfully applied to two-dimensional (2D) spin models [18] and quasi-one-dimensional fermionic ladder systems [19,20]. However, their applications to 2D fermionic systems are just beginning [13,21]. The results of the variational Monte Carlo method depend on the input trial wave functions [22]. The auxiliary field quantum Monte Carlo (QMC) method [23,24] is unbiased,

but it suffers from the notorious sign problem when doping away from half filling [25]. Once the sign problem occurs, the numeric errors grow exponentially as enlarging the system size and lowering the temperature, which usually plagues simulations, corresponding to a regime of maximal numerical difficulty in computational science for decades [11].

Recently, progress has appeared to employ the auxiliary field QMC method to study a spin-fermion model [26], which describes the low energy hot-spot fermionic excitations and yields the *d*-wave-like pairing symmetry [27]. This model is designed to be sign-problem free based on the previously proved Kramers-invariant decomposition by one of the authors and Zhang [28]. In such a decomposition, the Hubbard-Stratonovich (HS) transformation to fermion interactions is formulated in a Kramers invariant way, i.e., the fermion matrix in any HS field configuration satisfying the Kramers symmetry. Its determinant, working as the statistical weight, is a product of complex-conjugate pairs and thus positive definite. Developments along this line mainly follow the hot-spot dominated pairing mechanism [29–31]. However, these models begin with a metallic normal state far away from the Mott physics. For microscopic models such as the Hubbard-like ones exhibiting Mott physics at half filling, QMC simulations contribute significantly to the study of pairing mechanisms [32,33]; nevertheless, they often suffer from the notorious sign problem upon doping. It is desirable to simulate the emergence of superconductivity by doping Mott insulators through QMC simulations in a sign-problem free way.

In this article, we investigate the competition between antiferromagnetism and superconductivity by doping the parent
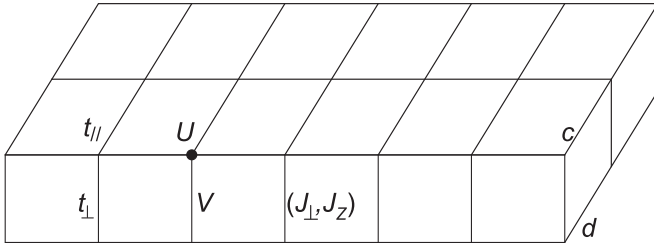

FIG. 1. Generalized SZH model is defined on a bilayer square lattice. Its parameters include the intra- and interlayer hoppings of $t_\parallel$ and $t_\perp$, respectively, the on-site Hubbard interaction U, the interactions between two sites along each rung with V in the charge channel, and $J_\perp$ and J_z of the AF superexchanges along the $x(y)$ and z directions, respectively.

2D Mott insulators. As an effective model, we employ the Scalapino-Zhang-Hanke (SZH) model by generalizing it to a bilayer version. It is a Hubbard-like model augmented by charge and spin-exchange interactions across each rung consisting of two sites. The explicit spin exchange favors both AF and SC, and thus provides a platform to study their competition, reminicient of the t-J model. The advantage of the SZH model is that, in a wide range of interaction parameters, it satisfies the criterion of the Kramers invariant decomposition for QMC simulations [28] and hence is sign-problem free at arbitrary electron fillings. This enables the possibility to study the transition from the AF insulating state to the SC state in a numerically exact manner; that is, any accuracy can be achieved within a polynomial time. At half filling, the ground state is either an AF insulator in the case with the Ising anisotropy or a rung-singlet Mott phase with the SU(2) invariance. Upon hole doping, the AF ordering is weakened and finally suppressed when the doping level $x > x_c \approx 0.11$. Meanwhile, the extended s-wave SC order grows up away from half filling and coexists with the AF order at $0 < x < x_c$.

II. MODEL AND QMC SIMULATIONS

The SZH model [34], originally defined for a two-leg ladder, is an extended Hubbard model for studying competing orders. We further generalize it to a bilayer square lattice as sketched in Fig. 1,

$$
\begin{aligned}
H = &-t_\parallel \sum_{\langle ij \rangle \sigma} (c_{i\sigma}^\dagger c_{j\sigma} + d_{i\sigma}^\dagger d_{j\sigma} + \text{H.c.}) \\
&- t_\perp \sum_{i\sigma} (c_{i\sigma}^\dagger d_{i\sigma} + \text{H.c.}) - \mu \sum_{i\sigma} (c_{i\sigma}^\dagger c_{i\sigma} + d_{i\sigma}^\dagger d_{i\sigma}) \\
&+ \frac{J_\perp}{2} \sum_i (S_{ic}^+ S_{id}^- + \text{H.c.}) + J_z \sum_i S_{ic}^z S_{id}^z \\
&+ U \sum_i \left[\left(n_{i\uparrow c} - \frac{1}{2} \right) \left(n_{i\downarrow c} - \frac{1}{2} \right) \right. \\
&\left. + \left(n_{i\uparrow d} - \frac{1}{2} \right) \left(n_{i\downarrow d} - \frac{1}{2} \right) \right] \\
&+ V \sum_i (n_{ic} - 1)(n_{id} - 1),
\end{aligned} \tag{1}
$$

where the electron annihilation operators in the upper and lower layers are denoted as c and d, respectively. Equation (1) consists of the intra- and interlayer nearest-neighboring hopping terms of $t_\parallel$ and $t_\perp$, respectively, and $t_\parallel$ is the energy unit set as 1. The interaction terms include the on-site Hubbard interaction U and the interactions between two sites along each vertical rung: V is the charge channel interaction; $J_\perp$ and J_z are the transverse and longitudinal spin exchanges, respectively. The in-plane AF correlation is intermediated through the second order perturbation theory. For the isotropic case with $J_\perp = J_z$, the system enters the rung singlet phase at half filling when the superexchange interaction across each rung is larger than the in-plane one which is perturbatively small. We first consider the case with the Ising anisotropy by setting $J_z > J_\perp$, which stabilizes the AF long-range order along the z direction at half filling. The AF parent insulating state is then doped for achieving the SC phase.

We will use Eq. (1) for studying a hard-core strong correlation problem in 2D on how superconductivity emerges by doping Mott insulators. The major advantage is that such a model will be later shown to be QMC sign-problem free in a large parameter region; hence it can be studied in a numerically exact way. Furthermore, it can be mapped to a monolayer two-orbital model [35,36] with the two orbitals equivalent to the upper and lower layers, respectively. Multiorbital models have been widely studied in strongly correlated systems such as iron-based superconductors [37]. It can also be mapped to a spin-$\frac{3}{2}$ fermionic Hubbard model [28,38–40] by defining $\psi_i = [c_{i\uparrow}, c_{i\downarrow}, d_{i\uparrow}, d_{i\downarrow}]^t$,

$$
\begin{aligned}
H = &-t_\parallel \sum_{\langle ij \rangle} (\psi_i^\dagger \psi_j + \text{H.c.}) - t_\perp \sum_i \psi_i^\dagger \Gamma^5 \psi_i - \mu \sum_i n_i \\
&- \sum_i \frac{g_c}{2} (n_i - 2)^2 - \sum_{i,a=1-5} \frac{g_a}{2} (n_i^a)^2,
\end{aligned} \tag{2}
$$

where

$$
n_i = \psi_i^\dagger \psi_i, \quad n_i^a = \frac{1}{2} \psi_i^\dagger \Gamma^a \psi_i, \tag{3}
$$

and the five Γ matrices are the rank-2 Clifford algebra, satisfying $\{\Gamma^a, \Gamma^b\} = 2\delta_{ab}$ with $1 \leqslant a < b \leqslant 5$, as defined in Appendix 1 following the convention in Ref. [38]. The interaction parameters in the two different representations of Eq. (1) and Eq. (2) are related by

$$
\begin{aligned}
4g_c &= \frac{J_\perp}{2} + \frac{J_z}{4} - U - 3V, \\
g_{1,5} &= \frac{J_\perp}{2} + \frac{J_z}{4} - U + V, \\
g_{2,3} &= \frac{J_\perp}{2} - \frac{J_z}{4} + U - V, \\
g_4 &= -\frac{J_\perp}{2} + \frac{3J_z}{4} + U - V.
\end{aligned} \tag{4}
$$

In Eq. (2), all the interaction terms are expressed in Kramers invariant operators n_i and n_i^a, which satisfy

$$
\mathcal{T} n_i \mathcal{T}^{-1} = n_i, \quad \mathcal{T} n_i^a \mathcal{T}^{-1} = n_i^a, \tag{5}
$$

and the Kramers transformation is defined as $\mathcal{T} = \Gamma^1 \Gamma^3 \mathcal{C}$ ($\mathcal{C}$ means complex conjugate). $\mathcal{T}$ is the usual time-reversal

transformation followed by switching the upper and lower layers.

When all the coupling constants g_c and g_a ($1 \leqslant a \leqslant 5$) are non-negative, the HS decomposition can be performed in a Kramers invariant way, such that the auxiliary field QMC is free of the sign problem [28,38–40]. The discrete HS decomposition for the four-fermion interaction is performed in an exact way as shown in Appendix 2. Roughly speaking, g_c favors the charge-density-wave (CDW) order and $g_{1,5}$ favors the rung current or bond-wave order, respectively [39], while $g_{2,3,4}$ favors the AF order. For simplicity, we set $g_c = g_1 = g_5 = 0$ for studying the antiferromagnetism-superconductivity transition. In practice, we have chosen $U = \frac{5}{2}$, $J_\perp = 1$, $J_z = 8$, $V = t_\perp = 0$, corresponding to $g_4 = 8g_2 = 8g_3 = 8$. Our QMC simulations employ the projector scheme working at zero temperature with the projection time $\beta = 4L$ and the discrete imaginary time slice $\Delta\tau = 0.1$. The results show convergences with respect to β and $\Delta\tau$ as shown in Appendix 3, respectively [41].

III. QMC RESULTS

We have performed QMC calculations on $2 \times L \times L$ lattices with L up to 12. A larger size with $L > 12$ is technically difficult because of the complicated matrix structures for the general interaction parameters, which significantly reduces the efficiency of the fast update algorithm [42], even though our results show clearly a transition from the half filled AF insulating phase to the singlet SC phase upon doping.

We first present the QMC simulation results of the structure factors, defined as the equal-time correlations, $F(\mathcal{O}) = L^2 \langle \mathcal{O}^\dagger \mathcal{O} \rangle$, where $\mathcal{O}$ represents a physical observable. In the magnetic channels, $\mathcal{O}$ is chosen as

$$N_z = \frac{1}{L^2} \sum_i n_i^4 (-1)^i, \quad N_{x(y)} = \frac{1}{L^2} \sum_i n_i^{2(3)} (-1)^i \quad (6)$$

for the AF order along the z direction (AF$_z$) and that along the $x(y)$ direction (AF$_{x(y)}$), respectively. Their structure factors F_{AF_z} and $F_{AF_{x(y)}}$ are shown in Figs. 2(a) and 2(b), respectively. The structure factors of AF$_z$ increase significantly versus L at $x < x_c \approx 0.11$, indicating the tendency for ordering. In contrast, those of AF$_{x(y)}$ nearly exhibit no size dependence, showing the absence of long-range order. For the SC channel, we have examined the extended s-wave singlet pairing order defined as $\Delta(i) = \frac{1}{\sqrt{2}L^2} \sum_i (c_{i\uparrow} d_{i\downarrow} - c_{i\downarrow} d_{i\uparrow})$, i.e., the pairing across each rung. Its structure factor F_{SC} increases with enlarging the sample size as shown in Fig. 2(c). If expressed with the bonding and antibonding band operators, $f_\alpha^{e(o)}(i) = \frac{1}{\sqrt{2}} [c_\alpha(i) \pm d_\alpha(i)]$, this pairing order parameter exhibits opposite signs on the $f^{e,o}$ bases as

$$\Delta(i) = \frac{1}{\sqrt{2}} [f_\uparrow^e(i) f_\downarrow^e(i) - f_\uparrow^o(i) f_\downarrow^o(i)]. \quad (7)$$

Hence it is an extended s-wave pairing order parameter. We have also measured the SC correlation within the layers, but it is much (several orders) smaller than the interlayer one. Hence, in the following, only the pairing across each rung will be considered. The extended s-wave pairing symmetry is among the promising candidates for the iron-based supercon-
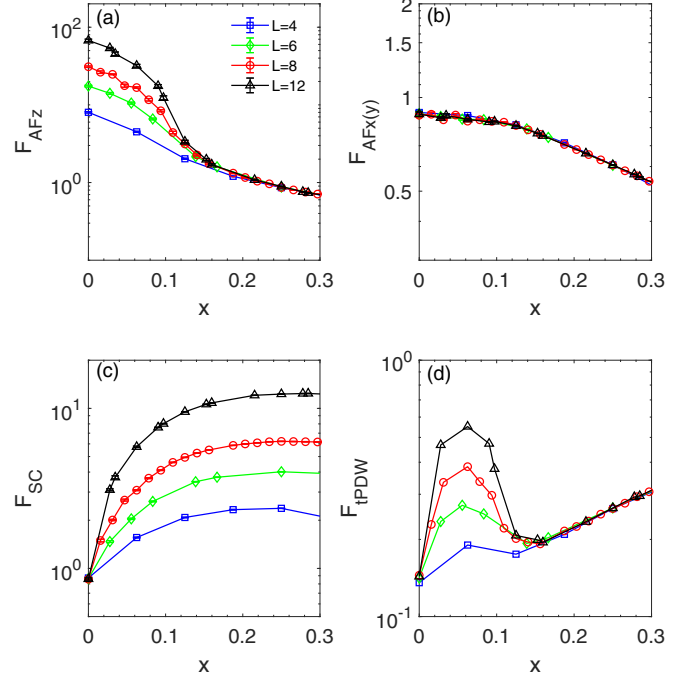

FIG. 2. QMC simulation results for the structure factors of (a) AF$_z$, (b) AF$_{x(y)}$, (c) SC, and (d) tPDW versus the doping x as varying L. In the disordered phase for each order parameter, each structure factor shows very small size dependence when $L \gg \xi$ and converges to a value proportional to the square of correlation length ξ^2, while, in the ordered phase, it grows as $L \to \infty$.

ductors [43]. In addition, a triplet pair-density wave (tPDW) correlation is found, whose order parameter is defined as

$$O_{tPDW} = \frac{1}{\sqrt{2}L^2} \sum_i (c_{i\uparrow} d_{i\downarrow} + c_{i\downarrow} d_{i\uparrow})(-1)^i. \quad (8)$$

It tends to develop ordering at $0 < x < x_c$ even though its magnitudes are small, as shown in Fig. 2(d).

Next we perform the finite-size scaling for these structure factors to extract the values of orderings in the thermodynamic limit as shown in Fig. 3 [44]. It is based on the scaling hypothesis $F(L)/L^2 = a + b/L + c\xi^2/L^2$ [45], and such a scaling method and its generalizations to general polynomials are widely used in literature [46–48].

At half filling ($x = 0$), only the AF$_z$ order exhibits a long-range ordering, while the SC order extrapolates to zero. At a small doping level with $x = \frac{1}{16}$, the AF$_z$ order still survives but its value is suppressed accompanied by the emerging of the SC order. As the doping level x increases to $\frac{1}{8}$ and above, the AF$_z$ order vanishes, leaving a pure rung-singlet SC order. The existences of the SC and AF$_z$ long-range orders are also evidenced by checking the decay patterns of the two-point correlation functions in real space as shown in Appendix 4. In fact, their coexistence is widely seen experimentally such as in various heavy fermion systems [49,50]. All the above results are summarized in the phase diagram as shown in Fig. 4. The AF$_z$ order exists in the region of $0 < x < x_c$ with $x_c \approx 0.11$ and the SC order appears immediately upon doping starting from zero.
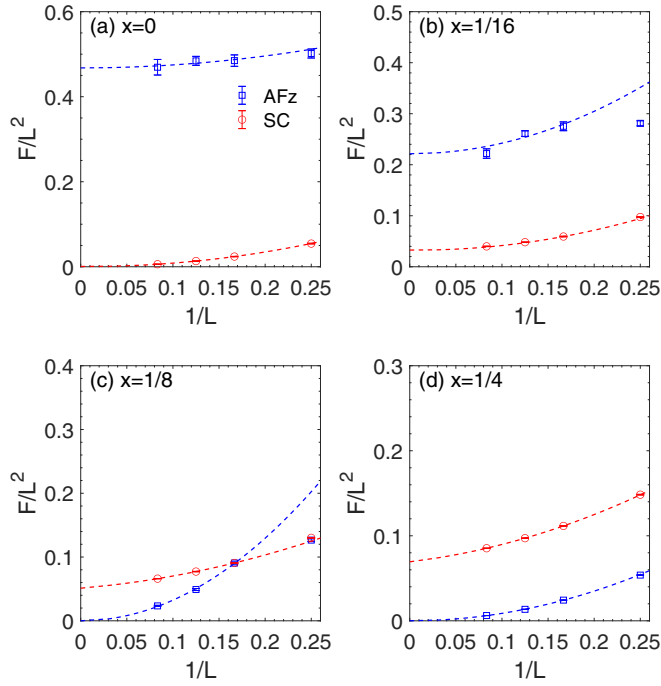
FIG. 3. Structure factors F/L^2 vs $1/L$ for both the AF$_z$ and SC orders. They are plotted at (a) $x = 0$, (b) $x = \frac{1}{16}$, (c) $x = \frac{1}{8}$, and (d) $x = \frac{1}{4}$, respectively. The dashed lines are polynomial fittings to the QMC data from $L = 6$ to $L = 12$.
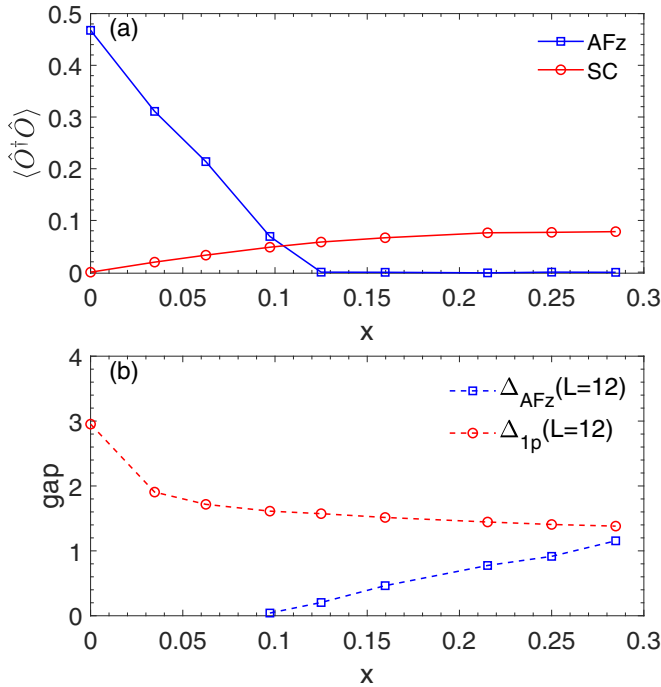

FIG. 4. (a) Extrapolation of $F/L^2 = \langle O^\dagger O \rangle$ in the limit of $L \to \infty$ versus x, where O represents operators for the AF$_z$, and SC order parameters. The AFz ordering is suppressed beyond a critical doping $x_c \approx 0.11$ and the SC order coexists with the AF$_z$ one at small dopings $0 < x < x_c$. (b) The single particle gap Δ_{1p} at all doping levels and the spin gap Δ_{AF_z} at $x > x_c$.
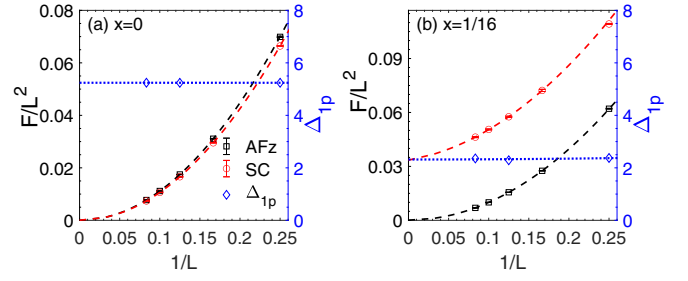

FIG. 5. QMC simulations for the SU(2) symmetric model. The finite size scalings of the structure factors F/L^2 of the AF and SC orders, and the single-particle gap Δ_{1p} at half filling (a) and the 1/16 doping (b). The scales for Δ_{1p} are along the axes on the right side of (a) and (b).

An interesting observation shown in Fig. 2(d) is that the tPDW tends to develop within $0 < x < x_c$, where the AF$_z$ and SC orders coexist. Based on the symmetry principle, there exists a coupling among these three orders constructed as $L_{tpdw} = g(N_z \Delta^\dagger O_{tPDW} + \text{H.c.})$, where g is an effective coupling constant. In the coexistence regime, where both N_z and Δ are finite, they combine as an external field to induce the tPDW order although its magnitude is too weak for an accurate identification. Similar to the SO(5) theory [9], the transition from the AF$_z$ ordering state to the SC state can be unified by a hidden SO(3) algebra structure: the total particle number N, O_{tPDW}, and $O^\dagger_{tPDW}$ form the generators of a pseudospin SO(3) group. Recently, the pair-density wave, either static or fluctuating, has received considerable attention due to its potential relation to the CDW and nematic orders in the pseudogap region of high T_c cuprates [10,51–54].

We next study the excitation gaps by calculating the imaginary-time-displaced correlation functions

$$\chi(\tau) = \langle T_\tau O(\tau) O^\dagger(0) \rangle, \qquad (9)$$

where T_τ means time ordering. The long-time behavior of $\chi(\tau)$ is related to the excitation gap Δ_O. As explained in Appendix 5, we measure the mean gap defined as $\Delta_O = (E_O + E_{O^\dagger} - 2E_0)/2$, where E_0 is the ground state energy and E_O ($E_{O^\dagger}$) gives the lowest energy excited by $O(O^\dagger)$. This gap can be extracted from $\chi(\tau)\chi(-\tau) \sim e^{-2\Delta_O \tau}$ for $\tau \to \infty$. For the single-particle gap, O is chosen as ψ_α with $\alpha = 1$–4, which yields the diagonal terms of the single-particle Green's function $G_{\alpha\alpha}(\tau)$. We use the averaged results of $G_{\alpha\alpha}(\tau)$ to yield the single-particle gap Δ_{1p} as plotted in Fig. 4(b). In the whole phase diagram, the single-particle excitations are all gapped and Δ_{1p} reaches the order of the band width in the AF order dominated region, indicating the existence of a Mott gap. We also calculate the spin gap Δ_{AF_z} associated with $O = N_z$ in the spin disordered region, which is also plotted in Fig. 4(b). It grows up at $x > x_c$ consistent with the vanishing of the AF$_z$ order.

We briefly discuss the consequence if the SU(2) symmetry is preserved. The QMC simulations are performed by setting $g_{2,3,4} = \frac{16}{3}$ and also $g_c = g_{1,5} = 0$, which corresponds to the case of $U = 4$, $J_\perp = J_z = \frac{16}{3}$, $V = t_\perp = 0$. The finite-size scalings of the AF and SC structure factors as well as the single-particle gap Δ_{1p} at half filling and at $x = \frac{1}{16}$ are presented in Figs. 5(a) and 5(b), respectively. The ground state

at half filling is a Mott insulator as shown in the nonzero single-particle gap Δ_{1p} and the vanishing AF ordering extrapolated to the thermodynamic limit. Quantum fluctuations are stronger in the SU(2) case than in the previously studied Ising anisotropic one; hence the system is a valence-bond-solid phase without symmetry breaking, i.e., the rung-singlet state. After doping, the SC long-range order is established in the absence of the AF order, as shown in Fig. 5(b), which is the same as the Ising case.

IV. SUMMARY

In summary, we have performed the projector QMC simulation based on the auxiliary field method on the bilayer SZH model, which is free of the sign problem. A quantum phase transition occurs from an Ising anisotropic AF insulating phase or an SU(2) invariant Mott insulating phase without the AF ordering to a rung-singlet SC phase with an extended *s*-wave symmetry driven by doping. In the coexistence regime between the AF_z and SC orders, their coupling leads to an enhanced tPDW correlation as a consequence of the symmetry principle. This work provides a reliable reference point for studying superconductivity and other competing orders by doping Mott insulators. Furthermore, the present study can be generalized to other bilayer geometries such as honeycomb or triangular lattices which may be relevant to certain materials and are left as future works.

APPENDIX

We present the detailed information about the model Hamiltonian and the quantum Monte Carlo (QMC) method, including the definition of Γ matrices, the projector QMC algorithm, the scalings of $\Delta\tau$ and β, the calculation of excitation gaps, and the spatial correlations.

1. Definition of Γ matrices

Following the convention in Ref. [38], we define the five Γ matrices as follows:

$$\Gamma^1 = \begin{pmatrix} 0 & -iI \\ iI & 0 \end{pmatrix}, \quad \Gamma^{2,3,4} = \begin{pmatrix} \vec{\sigma} & 0 \\ 0 & -\vec{\sigma} \end{pmatrix},$$

$$\Gamma^5 = \begin{pmatrix} 0 & I \\ I & 0 \end{pmatrix}, \tag{A1}$$

where I and $\vec{\sigma}$ are the 2×2 unit and Pauli matrices. They satisfy the anticommutation relation of

$$\{\Gamma^a, \Gamma^b\} = 2\delta_{ab}. \tag{A2}$$

Their commutators give rise to the 10 generators of the Sp(4) group as

$$\Gamma^{ab} = -\frac{i}{2}[\Gamma^a, \Gamma^b] \quad (1 \leqslant a, b \leqslant 5). \tag{A3}$$

The identity matrix, Γ^a $(1 \leqslant a \leqslant 5)$ and $\Gamma^{ab}(1 \leqslant a < b \leqslant 5)$ span the complete basis for the 16 bilinear operators in the particle-hole channel for four-component fermions defined as

$$n_i = \psi_{i,\alpha}^{\dagger} \psi_{i,\alpha},$$

$$n_i^a = \tfrac{1}{2}\psi_{i,\alpha}^{\dagger} \Gamma_{\alpha\beta}^a \psi_{i,\beta},$$

$$L_i^{ab} = -\tfrac{1}{2}\psi_{i,\alpha}^{\dagger} \Gamma_{\alpha\beta}^{ab} \psi_{i,\beta}. \tag{A4}$$

In the context of the bilayer model in the main text, we have

$$n_i = c_{i\sigma}^{\dagger} c_{i\sigma} + d_{i\sigma}^{\dagger} d_{i\sigma},$$

$$n_i^1 = -\frac{i}{2}(d_{i\sigma}^{\dagger} c_{i\sigma} - \text{H.c.}),$$

$$n_i^5 = \tfrac{1}{2}(d_{i\sigma}^{\dagger} c_{i\sigma} + \text{H.c.}),$$

$$n_i^{2,3,4} = c_{i,\alpha}^{\dagger}\left(\frac{\vec{\sigma}}{2}\right)_{\alpha\beta} c_{i\beta} - d_{i,\alpha}^{\dagger}\left(\frac{\vec{\sigma}}{2}\right)_{\alpha\beta} d_{i\beta}, \tag{A5}$$

where n_i is the total particle number on the rung, n_i^1 and n_i^5 are the bond current and bond strength along the rung, respectively, and $n^{2,3,4}$ are the bond Néel order. We define the Kramers symmetry as

$$\mathcal{T} = \Gamma^1 \Gamma^3 C, \tag{A6}$$

where C is the complex conjugate. Physically, $\mathcal{T}$ is the combination of the usual time-reversal transformation and the flipping of the upper and lower layers. It is easy to check that the above six bilinear operators are even under this Kramers operations.

The other 10 bilinear operators are odd under $\mathcal{T}$, which can be organized as

$$\text{Re}\vec{\pi}_i = c_{i\alpha}^{\dagger}\left(\frac{\vec{\sigma}}{2}\right)_{\alpha\beta} d_{i\beta} + \text{H.c.},$$

$$\text{Im}\vec{\pi}_i = -i\left[c_{i\alpha}^{\dagger}\left(\frac{\vec{\sigma}}{2}\right)_{\alpha\beta} d_{i\beta} - \text{H.c.}\right],$$

$$\bar{S}_i = c_{i,\alpha}^{\dagger}\left(\frac{\vec{\sigma}}{2}\right)_{\alpha\beta} c_{i\beta} + d_{i,\alpha}^{\dagger}\left(\frac{\vec{\sigma}}{2}\right)_{\alpha\beta} d_{i\beta},$$

$$Q_i = \tfrac{1}{2}(c_{i\sigma}^{\dagger} c_{i\sigma} - d_{i\sigma}^{\dagger} d_{i\sigma}), \tag{A7}$$

where $\text{Re}\vec{\pi}_i$ is the spin-channel bonding strength, $\text{Im}\vec{\pi}_i$ is the spin current along the rung, $\bar{S}_i$ is the total spin of the rung, and Q_i is the charge-density-wave order of the rung.

2. Projector QMC algorithm

We adopt the projector determinant QMC method [42] to study the model Hamiltonian shown in Eq. (1) in the main text. The basic idea is to apply the projection operator $e^{-\beta H/2}$ on a trial wave function $|\Psi_T\rangle$. If $\langle\Psi_G|\Psi_T\rangle \neq 0$ and there exists a nonzero gap between $|\Psi_G\rangle$ and the first excited state, $|\Psi_G\rangle$ is arrived at as the projection time $\beta \to \infty$,

$$|\Psi_G\rangle = \lim_{\beta\to\infty} e^{-\beta H/2}|\Psi_T\rangle, \tag{A8}$$

where the projection time β can be divided into M slices with $\beta = M\Delta\tau$, and the trial wave function can be written by filling N_e electrons,

$$|\Psi_T\rangle = \prod_i \sum_{j=1}^{N_e} c_j^\dagger P_{ji} |0\rangle. \quad (A9)$$

Here i, j contains both site and flavor indices and $|0\rangle$ labels the fermion vacuum. In practice, $|\Psi_T\rangle$ can be chosen as the ground state of a free fermion Hamiltonian. The scattering matrix $\langle\Psi_T|e^{-\beta H}|\Psi_T\rangle$ is obtained by integrating out the fermionic degrees of freedom,

$$\langle\Psi_T|e^{-\beta H}|\Psi_T\rangle = \sum_{\{\sigma\}} \left[\prod_i \gamma_i(\sigma_i)\right] \det(P^\dagger B_L B_{L-1} \ldots B_1 P), \quad (A10)$$

where σ_i labels the auxiliary discrete boson field (see below). The scattering matrix Eq. (A10), which plays the role of the partition function, serves as the basis of the projector determinant QMC algorithm. The $\{\sigma_i\}$ fields are then sampled by using the standard Monte Carlo technique.

In order to obtain Eq. (A10), two preliminary steps are needed. The second order Suzuki-Trotter decomposition

$$e^{-\Delta\tau(K+V)} = e^{-\Delta\tau K/2} e^{-\Delta\tau V} e^{-\Delta\tau K/2} + o[(\Delta\tau)^3] \quad (A11)$$

is first used to separate the kinetic (K) and interaction (V) terms in each time slice, and then the $e^{-\Delta\tau V}$ term is decoupled by using the discrete Hubbard-Stratonovich transformation,

$$e^{gX^2} = \sum_{\sigma=\pm 1,\ldots,\pm I_{\max}} \gamma(\sigma) e^{\lambda(\sigma)X}, \quad (A12)$$

where σ is the discrete Hubbard-Stratonovich field. If eigenvalues $\mathrm{eig}(X) = \{0, \pm 1\}$, the maximal value of σ, I_{max} can be set as 1 [23] along with the choices of $\gamma(\sigma)$ and $\lambda(\sigma)$ as

$$\gamma(\pm 1) = \tfrac{1}{2}, \quad \lambda(\pm 1) = \pm\cosh^{-1}(e^g). \quad (A13)$$

If $\mathrm{eig}(X) = \{0, \pm 1, \pm 2, \pm 3\}$, we need to set $I_{\max} = 2$ and choose

$$\gamma(\pm 1) = \frac{-a(3+a^2)+d}{4d},$$

$$\gamma(\pm 2) = \frac{a(3+a^2)+d}{4d},$$

$$\eta(\pm 1) = \pm\cosh^{-1}\left\{\frac{a+2a^3+a^5+(a^2-1)d}{4}\right\},$$

$$\eta(\pm 2) = \pm\cosh^{-1}\left\{\frac{a+2a^3+a^5-(a^2-1)d}{4}\right\},$$

$$(A14)$$

where $a = e^g$ and $d = \sqrt{8+a^2(3+a^2)^2}$ [55]. In our case, $X = \psi^\dagger \Gamma^{2,3,4}\psi$, whose eigenvalues are among $0, \pm 1, \pm 2$; hence the latter Hubbard-Stratonovich transformation is applied.

3. $\Delta\tau$ and β scalings

In the projector QMC algorithm, the systematic error mainly comes from two origins: the finite time step $\Delta\tau$ and
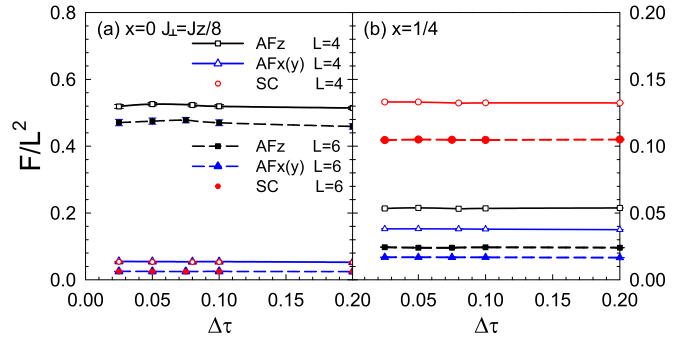

FIG. 6. $\Delta\tau$ dependence of the structure factors for various order parameters for $x = 0$ (a) and $x = \frac{1}{4}$ (b) with $L = 4$ (solid lines) and $L = 6$ (dashed lines). AF$_z$ and AF$_{x(y)}$ represent the antiferromagnetic order along the z direction and that along the x or y direction, respectively, and SC represents the superconducting order. The interacting parameter values are $U = 2.5$, $V = t_\perp = 0$, $J_\perp = 1$, and $J_z = 8$.

the finite projection time β. In the following, we perform the error analysis on both $\Delta\tau$ and β. In this section, we employ the parameter values for $U = 2.5$, $J_\perp = 1$, $J_z = 8$, $V = t_\perp = 0$ for simulations below.

For the Suzuki-Trotter decomposition defined in Eq. (A11), detailed calculation shows that its error is at the order of $\max\{tg_i^2, t^2 g_i\}(\Delta\tau)^3$. In Fig. 6, scalings of the antiferromagnetic structure factors along the z, $x(y)$ directions and the superconductivity structure factor vs $\Delta\tau$ are plotted for $x = 0$ in (a) and $x = \frac{1}{4}$ in (b). The slopes of these scaling lines are nearly independent on the lattice size L for all three orders. Therefore, we only need to check the small lattice size. Due to the convergence of the finite $\Delta\tau$ scaling, we use the value of $\Delta\tau = 0.1$ in all the simulations.

We further check the effect of the finite projection time β. In Fig. 7, the scalings of the antiferromagnetic structure factors along the z and $x(y)$ directions and the superconducting structure factor vs β are presented. For each curve, β_c is defined as the convergence projection time after which the structural factors converge. It is shown that the antiferromagnetic order parameter along the $x(y)$ direction and the superconducting order parameter converge very quickly for both $x = 0$ and $x = 1/4$. The corresponding β_c is found to be

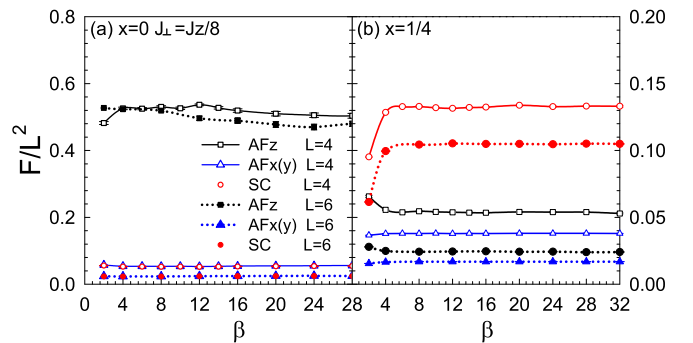FIG. 7. β dependence of structure factors of various order parameters for $x = 0$ (a) and $x = \frac{1}{4}$ (b) with $L = 4$ (solid lines) and $L = 6$ (dashed lines). The symbols and the interacting parameter values are the same as those presented in Fig. 6.
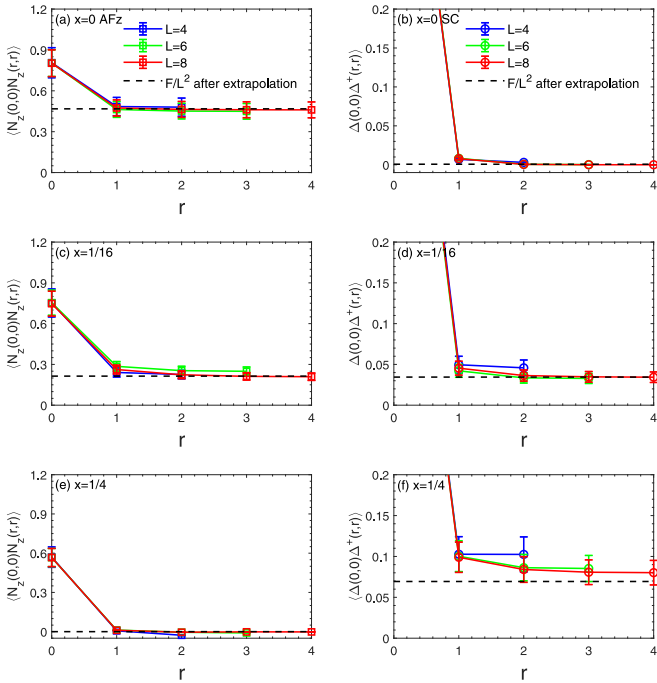
FIG. 8. Spatial correlation functions at different doping levels with system size $L = 4$, 6, and 8. The correlation functions for the AF_z and SC orders at $x = 0$ are plotted in (a) and (b), respectively; those at $x = 1/16$ are plotted in (c) and (d) ($x = 1/18$ for the case of $L = 6$), respectively; those at $x = 1/4$ are plotted in (e) and (f), respectively. The squares of the order parameters obtained by the finite size scaling on the structure factors in the main text are plotted with dashed lines for comparison.

around 8. For the antiferromagnetic order along the z direction, we set $\beta_c = 16$, which should be enough for $L = 4$, and $\beta_c = 24$ for $L = 6$ as well. This indicates that $\beta_c(L) = 4L$ is safe for convergence, which is taken for all the simulations presented in the main text for accurate numeric results.

Simulations in the main text are performed on 20 cores for each group of parameters with 500 warm-up steps and more than 1000 steps of measurements.

4. Spatial correlations

To demonstrate the SC long-range order after doping and its coexistence with the AF_z order, we examine their spatial correlations $\langle O(0, 0)O^\dagger(r, r)\rangle$ [56]. The results are presented in Fig. 8 at three typical doping levels, i.e., $x = 0$, 1/16, and 1/4, which correspond to the cases with only the AF_z order, the coexistence of the AF_z and SC orders, and only the SC order, respectively. For the system size with $L = 6$, $x = 1/18$ is used instead due to its commensurability with the system.

For all of these doping levels, the spatial correlations saturate at large distances. As L increases, the farthest correlation
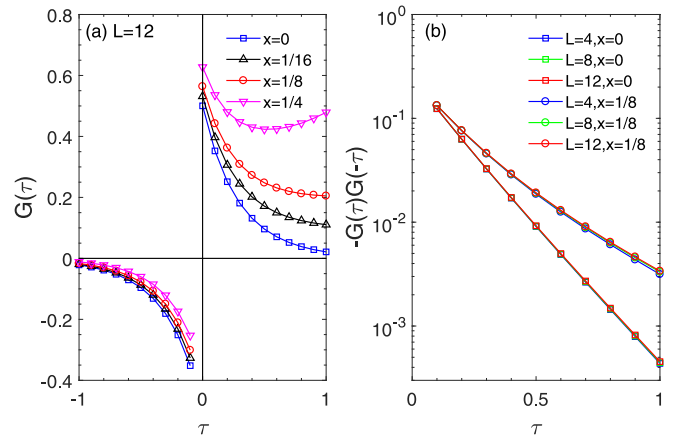

FIG. 9. Imaginary time Green's functions. $G(\tau)$ is plotted at different dopings. Due to the particle-hole symmetry at half filling, the relation of $G(\tau) = -G(-\tau)$ is satisfied, while this symmetry is not held away from half filling. We employ $[-G(\tau)G(-\tau)]$ to extract the mean single particle gap, plotted in (b), which shows very weak size dependence.

functions approach the values obtained via the finite-size scalings on the corresponding structure factors in the main text. The consistency between two approaches demonstrates that the long-range orderings of the AF_z and SC are reliable.

5. Calculation of excitation gaps

As explained in the main text, we calculate the spectra gap functions through the imaginary-time displaced correlation functions $\chi(\tau) = T_\tau \langle \mathcal{O}(\tau)\mathcal{O}^\dagger(0)\rangle$. Since our QMC works in the canonical ensemble, we can only obtain the energy difference directly through $\chi(\tau) \sim e^{-(E_{\mathcal{O}^\dagger} - E_0)\tau}$ for $\tau \to \infty$ and $\chi(\tau) \sim e^{(E_{\mathcal{O}} - E_0)\tau}$ for $\tau \to -\infty$, where E_0 is the ground state energy and $E_{\mathcal{O}}(E_{\mathcal{O}^\dagger})$ gives the lowest energy excited by $\mathcal{O}(\mathcal{O}^\dagger)$. On the other hand, the physical gap should take the chemical potential into account, i.e., $\Delta_{\mathcal{O}} = E_{\mathcal{O}} - E_0 - \mu N_{\mathcal{O}}$, where $N_{\mathcal{O}}$ is the particle number of the excited states. Nevertheless, the relation between particle number N and μ is generally complicated, especially for an interacting model. We use the average of $\Delta_{\mathcal{O}}$ and $\Delta_{\mathcal{O}^\dagger}$ as the excitation gap, in which μ does not appear explicitly.

In Fig. 9(a), we plot the single-particle Green's function $G(\tau)$ as an example to clarify our points. Only at half filling does $G(\tau)$ show the particle-hole symmetry, i.e., $G(\tau) = -G(-\tau)$. Away from the half filling, the particle-hole symmetry is broken. If we directly take the slope of $\log[G(\tau)]$ versus τ as the excitation gap, we even obtain a negative value, for example, at $x = 1/4$. According to the above discussions, we extract the mean gaps from $\log[-G(\tau)G(-\tau)]$, as shown in Fig. 9(b), which show very small size dependences.

[1] F. Steglich, J. Aarts, C. D. Bredl, W. Lieke, D. Meschede, W. Franz, and H. Schäfer, Phys. Rev. Lett. **43**, 1892 (1979).

[2] J. G. Bednorz and K. A. Müller, Z. Phys. B: Condens. Matter **64**, 189 (1986).

[3] Y. Kamihara, T. Watanabe, M. Hirano, and H. Hosono, J. Am. Chem. Soc. **130**, 3296 (2008).

[4] D. Jérome, A. Mazaud, M. Ribault, and K. Bechgaard, J. Phys. Lett. **41**, 95 (1980).

[5] S.-C. Zhang, Science **275**, 1089 (1997).

[6] S. Sachdev, Rev. Mod. Phys. **75**, 913 (2003); S. A. Kivelson, I. P. Bindloss, E. Fradkin, V. Oganesyan, J. M. Tranquada, A. Kapitulnik, and C. Howald, *ibid.* **75**, 1201 (2003); P. A. Lee, N. Nagaosa, and X.-G. Wen, *ibid.* **78**, 17 (2006).

[7] Z.-Y. Weng, Front. Phys. **6**, 370 (2011).

[8] X. Chen, P. Dai, D. Feng, T. Xiang, and F.-C. Zhang, Nat. Sci. Rev. **1**, 371 (2014).

[9] E. Demler, W. Hanke, and S.-C. Zhang, Rev. Mod. Phys. **76**, 909 (2004).

[10] E. Fradkin, S. A. Kivelson, and J. M. Tranquada, Rev. Mod. Phys. **87**, 457 (2015).

[11] B.-X. Zheng, C.-M. Chung, P. Corboz, G. Ehlers, M.-P. Qin, R. M. Noack, H. Shi, S. R. White, S. Zhang, and G. K.-L. Chan, Science **358**, 1155 (2017).

[12] E. W. Huang, C. B. Mendl, S. Liu, S. Johnston, H.-C. Jiang, B. Moritz, and T. P. Devereaux, Science **358**, 1161 (2017).

[13] H.-C. Jiang and T. P. Devereaux, Science **365**, 1424 (2019).

[14] D. J. Scalapino, Rev. Mod. Phys. **84**, 1383 (2012).

[15] E. Dagotto, Rev. Mod. Phys. **66**, 763 (1994).

[16] S. R. White, Phys. Rev. Lett. **69**, 2863 (1992).

[17] U. Schollwöck, Ann. Phys. **326**, 96 (2011), January 2011 Special Issue.

[18] E. Stoudenmire and S. R. White, Annu. Rev. Condens. Matter Phys. **3**, 111 (2012).

[19] L. Liu, H. Yao, E. Berg, S. R. White, and S. A. Kivelson, Phys. Rev. Lett. **108**, 126406 (2012).

[20] S. R. White, D. J. Scalapino, and S. A. Kivelson, Phys. Rev. Lett. **115**, 056401 (2015).

[21] P. Corboz, T. M. Rice, and M. Troyer, Phys. Rev. Lett. **113**, 046402 (2014).

[22] B. Edegger, V. N. Muthukumar, and C. Gros, Adv. Phys. **56**, 927 (2007).

[23] J. E. Hirsch, Phys. Rev. B **28**, 4059 (1983).

[24] R. Blankenbecler, D. J. Scalapino, and R. L. Sugar, Phys. Rev. D **24**, 2278 (1981).

[25] M. Troyer and U.-J. Wiese, Phys. Rev. Lett. **94**, 170201 (2005).

[26] A. Abanov and A. V. Chubukov, Phys. Rev. Lett. **84**, 5608 (2000).

[27] E. Berg, M. A. Metlitski, and S. Sachdev, Science **338**, 1606 (2012).

[28] C. Wu and S.-C. Zhang, Phys. Rev. B **71**, 155115 (2005).

[29] Y. Schattner, M. H. Gerlach, S. Trebst, and E. Berg, Phys. Rev. Lett. **117**, 097002 (2016).

[30] Z.-X. Li, F. Wang, H. Yao, and D.-H. Lee, Phys. Rev. B **95**, 214505 (2017).

[31] X. Wang, Y. Schattner, E. Berg, and R. M. Fernandes, Phys. Rev. B **95**, 174520 (2017).

[32] S. R. White, D. J. Scalapino, R. L. Sugar, E. Y. Loh, J. E. Gubernatis, and R. T. Scalettar, Phys. Rev. B **40**, 506 (1989).

[33] J. E. Hirsch, E. Loh, D. J. Scalapino, and S. Tang, Phys. Rev. B **39**, 243 (1989).

[34] D. Scalapino, S.-C. Zhang, and W. Hanke, Phys. Rev. B **58**, 443 (1998).

[35] T. A. Maier and D. J. Scalapino, Phys. Rev. B **84**, 180513(R) (2011).

[36] L. Rademaker, S. Johnston, J. Zaanen, and J. van den Brink, Phys. Rev. B **88**, 235115 (2013).

[37] G. R. Stewart, Rev. Mod. Phys. **83**, 1589 (2011).

[38] C. Wu, J.-p. Hu, and S.-c. Zhang, Phys. Rev. Lett. **91**, 186402 (2003).

[39] S. Capponi, C. Wu, and S.-C. Zhang, Phys. Rev. B **70**, 220505(R) (2004).

[40] C. Wu, Mod. Phys. Lett. B **20**, 1707 (2006).

[41] The choice of $\beta = 4L$ means that, as L increases, the projection time β increases accordingly, ensuring the ground state can be achieved for each L as the gap is roughly proportional to $1/L$.

[42] F. Assaad and H. Evertz, World-line and determinantal quantum monte carlo methods for spins, phonons and electrons, in *Computational Many-Particle Physics*, edited by H. Fehske, R. Schneider, and A. Weiße (Springer Berlin Heidelberg, Berlin, Heidelberg, 2008), pp. 277–356

[43] A. Chubukov, Annu. Rev. Condens. Matter Phys. **3**, 57 (2012).

[44] All the error bars have been added on figures, while some of them may be too tiny to be seen which are within the size of symbols.

[45] By assuming the spatial correlation $\langle O(\boldsymbol{r})O(\boldsymbol{0})\rangle = a + \frac{b}{4\pi r} + \frac{c}{8\pi}e^{-r/\xi}$, its Fourier transformation gives the scaling behavior of the structure factor shown in the main text, where a is the thermodynamic expectation value (square of the order parameter), the b term is the contribution from the gapless excitations (e.g., the Goldstone modes), and the c term represents the short-range correlations, or, the gapped excitations. For the AF$_z$ order, since there is no Goldstone mode, the b term is not needed. However, for the superconductivity, all three terms should be kept since there is no Anderson-Higgs mechanism to "eat" the gapless phase mode in our calculations.

[46] S. Sorella, Y. Otsuka, and S. Yunoki, Sci. Rep. **2**, 992 (2012).

[47] F. F. Assaad and I. F. Herbut, Phys. Rev. X **3**, 031010 (2013).

[48] T. Ma, L. Zhang, C.-C. Chang, H.-H. Hung, and R. T. Scalettar, Phys. Rev. Lett. **120**, 116601 (2018).

[49] T. Park, F. Ronning, H. Q. Yuan, M. B. Salamon, R. Movshovich, J. L. Sarrao, and J. D. Thompson, Nature (London) **440**, 65 (2006).

[50] B. D. White, J. D. Thompson, and M. B. Maple, Physica C **514**, 246 (2015).

[51] P. A. Lee, Phys. Rev. X **4**, 031017 (2014).

[52] B. Keimer, S. A. Kivelson, M. R. Norman, S. Uchida, and J. Zaanen, Nature (London) **518**, 179 (2015).

[53] Y.-M. Lu, T. Xiang, and D.-H. Lee, Nat. Phys. **10**, 634 (2014).

[54] L.-H. Chen, D. Wang, Y. Zhou, and Q.-H. Wang, Chin. Phys. Lett. **37**, 017403 (2020).

[55] D. Wang, Y. Li, Z. Cai, Z. Zhou, Y. Wang, and C. Wu, Phys. Rev. Lett. **112**, 156403 (2014).

[56] R. T. Clay, H. Li, and S. Mazumdar, Phys. Rev. Lett. **101**, 166403 (2008).